catalysts

MDPI

Article

Specific Immobilization of *Escherichia coli* Expressing Recombinant Glycerol Dehydrogenase on Mannose-Functionalized Magnetic Nanoparticles

Fei-Long Li [1,†], Meng-Yao Zhuang [1,†], Jia-Jia Shen [1], Xiao-Man Fan [1], Hyunsoo Choi [2], Jung-Kul Lee [2,*] and Ye-Wang Zhang [1,3,*]

1 School of Pharmacy, United Pharmaceutical Institute of Shandong Tianzhilvye Biotechnology Co. Ltd. and Jiangsu University, Zhenjiang 212013, China; feilongli2018@outlook.com (F.-L.L.); zhuang_mengyao@outlook.com (M.-Y.Z.); shenjiajia20@163.com (J.-J.S.); fanxiaomanmail@yeah.net (X.-M.F.)
2 Department of Chemical Engineering, Konkuk University, 1 Hwayang Dong, Seoul 05029, Korea; hyunsoo4062@naver.com
3 College of Petroleum and Chemical Engineering, Beibu Gulf University, Qinzhou 535011, China
* Correspondence: jkrhee@konkuk.ac.kr (J.-K.L.); zhangyewang@ujs.edu.cn (Y.-W.Z.); Tel.: +82-458-3504 (J.-K.L.); +86-511-8503-8201 (Y.-W.Z.)
† These authors contributed equally to this work.

Received: 16 November 2018; Accepted: 13 December 2018; Published: 24 December 2018

Abstract: Mannose-functionalized magnetic nanoparticles were prepared for the immobilization of *Escherichia coli* cells harboring the recombinant glycerol dehydrogenase gene. Immobilization of whole *E. coli* cells on the carrier was carried out through specific binding between mannose on the nanoparticles and the FimH lectin on the *E. coli* cell surface via hydrogen bonds and hydrophobic interactions. The effects of various factors including cell concentration, pH, temperature, and buffer concentration were investigated. High degrees of immobilization (84%) and recovery of activity (82%) were obtained under the following conditions: cell/support 1.3 mg/mL, immobilization time 2 h, pH 8.0, temperature 4°C, and buffer concentration 50 mM. Compared with the free cells, the thermostability of the immobilized cells was improved 2.56-fold at 37 °C. More than 50% of the initial activity of the immobilized cells remained after 10 cycles. The immobilized cells were evaluated functionally by monitoring the catalytic conversion of glycerol to 1,3-dihydroxyacetone (DHA). After a 12 h reaction, the DHA produced by the immobilized cells was two-fold higher than that produced by the free cells. These results indicate that mannose-functionalized magnetic nanoparticles can be used for the specific recognition of gram-negative bacteria, which gives them great potential in applications such as the preparation of biocatalysts and biosensors and clinical diagnosis.

Keywords: mannose; magnetic nanoparticles; immobilization; whole cell; specific recognition

1. Introduction

As important biocatalysts, bacteria are widely used in sewage treatment, environmental remediation, and the production of drugs, pharmaceutical intermediates, food processing, and industrial chemical products [1,2]. However, free bacterial cells are unstable, and their reusability in culture medium or in a reaction solution requires critical reaction conditions. Compared with free cells, the immobilized cells can be easily re-used, and extremely high bacterial levels can be readily obtained in bioreactors using them [3]. Thus, immobilization of whole cells is receiving increased attention because of its potential in biocatalysis [4,5].

Generally, immobilization techniques have been proven to enhance the properties of biocatalysts, including whole cells and enzymes [6–10]. Nanostructure materials have been used as drug carriers and in

other biological applications [11–17] and proved to have great potential in stabilizing cells, allowing their use for extended periods [18,19]. Among all nanomaterials, magnetic Fe_3O_4 nanoparticles have several advantages, including a large surface area, superparamagnetism, low toxicity, good biocompatibility, and ease of recycling [20,21]. Therefore, they are ideal for cell immobilization.

There are several widely used cell immobilization methods, including adsorption onto/into solid supports [22], entrapment in a matrix [23], cross-linking [24], and covalent binding to the carrier [25]. Of these methods, immobilization by adsorption has relatively slight influence on the biological activity of cells and often uses macroporous resins [26] or glass beads [27] as the immobilized carrier. However, weak binding and poor mechanical stability may cause cell leakage leading to a shortened utility lifespan [28]. Although the attachment of cells to supports using cross-linking or covalent binding reduces cell leakage, it is incompatible with cell viability since the cross-linking agents are highly toxic to microbial cells [29]. Recently, enzymes or active groups expressed on the cell surface have been reported [24,30]. However, it is difficult to express and control the orientation of heterologous proteins on the cell surface. Thus, the development of an appropriate immobilization method for bacterial cells remains an important goal.

It has been reported that gram-negative bacteria produce surface lectins which are usually presented in the form of filamentous pili, assembled from more than 1000 protein subunits [31,32]. As a typical gram-negative bacterial, *Escherichia coli* also produces cell surface lectins, and among these the most common is the FimH protein, which is comprised of 17 kDa subunits. These subunits have an extended trisaccharide binding site and preferentially bind oligomannose [33,34]. In the present study, we have developed a promising method for the immobilization of *E. coli* based on specific recognition between the FimH protein on the surface of bacteria and mannose-functionalized magnetic nanoparticles. These mannose-functionalized magnetic nanoparticles were fabricated (Scheme 1) and used as an effective carrier for the immobilization of *E. coli* cells expressing recombinant glycerol dehydrogenase, which was then used to synthesize 1,3-dihydroxyacetone (DHA) to investigate their biological activity (Scheme 2).

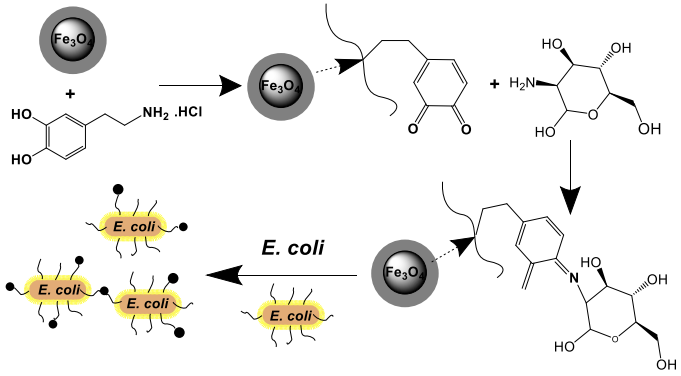

Scheme 1. Carrier preparation and *Escherichia coli* cell immobilization.

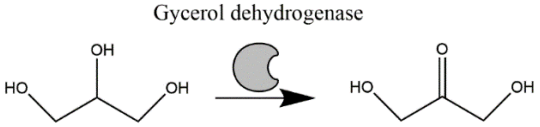

Scheme 2. Synthesis of 1,3-dihydroxyacetone (DHA) using *E. coli* expressing recombinant glycerol dehydrogenase.

2. Results and Discussion

2.1. Characterization of the Nanoparticles

The preparation of nanoparticles, including Fe_3O_4, Fe_3O_4@OA (oleic acid), and Fe_3O_4@OA@DP (dopamine), and the characterization of these nanoparticles using Fourier transform infrared spectroscopy (FTIR) and transmission electron microscopy (TEM) have been reported in our previous work [35]. To demonstrate that mannose was successfully anchored onto the surface of magnetic Fe_3O4@OA@DP, the nanoparticles were analyzed using FTIR. As shown in Figure 1, in the Fe_3O_4 FTIR spectra, the band at 580 cm^{-1} was assigned to the Fe–O vibration. Compared with the Fe_3O_4@OA@DP nanoparticles, new bands at 1400 and 1643 cm^{-1} appeared in the Fe_3O_4@OA@DP–mannose nanoparticles spectrum. This was due to the fact that the residual quinone functional groups on the nanoparticles were reactive toward the nucleophilic amino groups in mannosamine and could be covalently coupled to mannosamine with polydopamine through a Michael addition and Schiff base formation [34]. These results demonstrated that the mannose was successfully functionalized onto the magnetic Fe_3O_4@OA@DP nanoparticles.

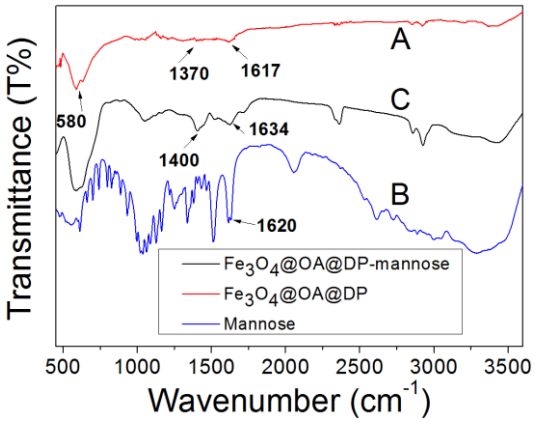

Figure 1. FTIR spectra of (**A**) Fe_3O_4@OA@DP, (**B**) mannose, and (**C**) Fe_3O_4@OA@DP–mannose.

The mannose-functionalized nanoparticles were then used to immobilize *E. coli* cells. To investigate the morphological changes and dispersional stabilization of the Fe_3O_4@OA@DP, Fe_3O_4@OA@DP–mannose, and Fe_3O_4@OA@DP–mannose–*E. coli* nanoparticles, transmission electron microscopy (TEM) was conducted (Figure 2). The average size of the Fe_3O_4@OA@DP nanoparticles (Figure 2A) was approximately 20 nm in diameter. After functionalization with mannose, the size of the Fe_3O_4@OA@DP–mannose (Figure 2B) particles became significantly larger than that of the Fe_3O_4@OA@DP nanoparticles, presenting an average diameter of 32 nm. From Figure 2C, it is clear that the *E. coli* cells were immobilized on the Fe_3O_4@OA@DP–mannose nanocarrier successfully. In previous reports, it was proven that there was no binding between mannose and *E. coli* lacking the FimH gene [36,37]. The specific recognition between the D-mannose-containing structure and *E. coli* containing the FimH gene was directly shown with receptor immuno-electron microscopy [38,39]. By adding a high concentration of D-mannose ammonium hydrochloride (100 mM), 95.2% of cells could be removed from the nanoparticles. This indicated that the interactions between FimH and mannose-functionalized nanoparticles were weaker than those between FimH and mannose monomers. This result is in agreement with the inhibition potency of mannosides with respect to the adhesion of *E. coli* to mannose-coated surfaces [40]. It has also been proven that the binding between mannose-containing magnetic nanoparticles is highly specific, which could be effective for the immobilization of *E. coli*.

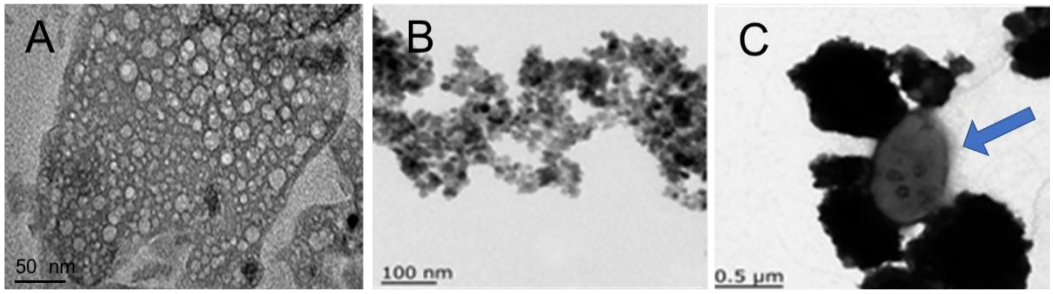

Figure 2. TEM of (**A**) Fe_3O_4@OA@DP, (**B**) Fe_3O_4@OA@DP-mannose, (**C**) Fe_3O_4@OA@DP–mannose–*E. coli*. The arrow indicates an immobilized *E. coli* cell.

2.2. Optimization of the Immobilization Conditions

In the present study, we utilized the specific binding between mannose and FimH lectin to immobilize *E. coli* cells expressing recombinant glycerol dehydrogenase onto magnetic nanoparticles. To achieve a high yield and biological activity of the cells, conditions such as pH, temperature, cell concentration, and buffer concentration were optimized. pH is an important factor for the immobilization of *E. coli* because the hydrogen bonds formed and the hydrophobic interactions involved in this process are highly dependent on it [33]. As shown in Figure 3A, the immobilization yield increased from 26.5% at pH 6.5 to the highest value of 82.4% at pH 8.0, but decreased sharply to 46.3% at pH 11. The recovery activity showed a similar tendency, which was 46.3% at pH 6, reaching the highest value of 85.1% at pH 9. Thereafter, it decreased to 73.6% at pH 10 and to 39.6% at pH 11. These results may be due to the fact that protons bind to the lone pair electrons on the amino N atom under acidic conditions. Under conditions of alkalinity (pH > 8.0), the protons on FimH lectin will likely be taken away by the hydroxide ions in the solution, leading to a destruction of the hydrogen bonds [41]. Thus, the optimal pH for immobilization was determined to be 8.0, on the basis of an evaluation of the immobilization yield and the recovery of activity.

The effect of cell concentration on the immobilization of *E. coli* was also examined (Figure 3B). The immobilization yield gradually decreased with the increase of cell concentration, with a yield as high as 100% at the lowest cell concentration of 4.55 mg/mL, whereas at the highest cell concentration of 25.5 mg/mL, the immobilization yield was only 64.33%. The reason for this might be that the number of nanoparticles was insufficient to immobilize all cells at high cell concentrations [42]. Unlike the immobilization yield, the activity recovery of the immobilized cells increased as cell concentration increased. At a cell concentration of 4.55 mg/mL, the activity recovery was only 31.45%, whereas it reached 92.74% when the cell concentration increased to 25.5 mg/mL. Based on the consideration of both the immobilization yield and activity recovery, a cell concentration of 13.45 mg/mL was selected for cell immobilization. The immobilization time was investigated from 0.25 to 2.0 h. After 2 h, the immobilization yield and the activity recovery reached their highest values at 82.4% and 82.5%, respectively. These values likely represent the dynamic balance between both adsorption and desorption [43,44].

Figure 3C shows the effect of temperature on the cells immobilized onto the functionalized Fe_3O_4@OA@DP nanoparticles. The optimal immobilization temperature was 4 °C. As the temperature increased, the immobilization yield and the activity recovery gradually decreased from 82.4 to 70.5% and 80 to 46%, respectively. When the temperature increases, secondary bonds within the enzyme structure are disrupted, which may lead to a change in the enzyme's conformation, resulting in a loss of cell activity. The Brownian motion between the molecules increases as well, which could further lead to the breakage of hydrogen bonds [45].

The effect of buffer concentration on the immobilization process was determined over the range 0.01 to 0.25 M (Figure 3D). The results indicated that the recovery of activity reached its highest value of 92% at a buffer concentration of 50 mM and then decreased with increasing buffer concentrations. Meanwhile, as the buffer concentration increased, the immobilization yield decreased.

The reason for this might be that a high buffer concentration affects the surface charge of the enzyme, removing its surface hydration layer, which would then affect the formation of hydrogen bonds [46]. The immobilization mechanism used here represents a highly specific recognition between mannose residues and the FimH protein. All the mannose hydroxyls, with the exception of the anomeric hydroxyl, interacted extensively with the binding domain residues in the FimH protein [47]. The amine groups at the N-terminal of the FimH protein interacted with the 2-OH, 6-OH, and the ring oxygen of the mannose moiety to form hydrogen bonds [48].

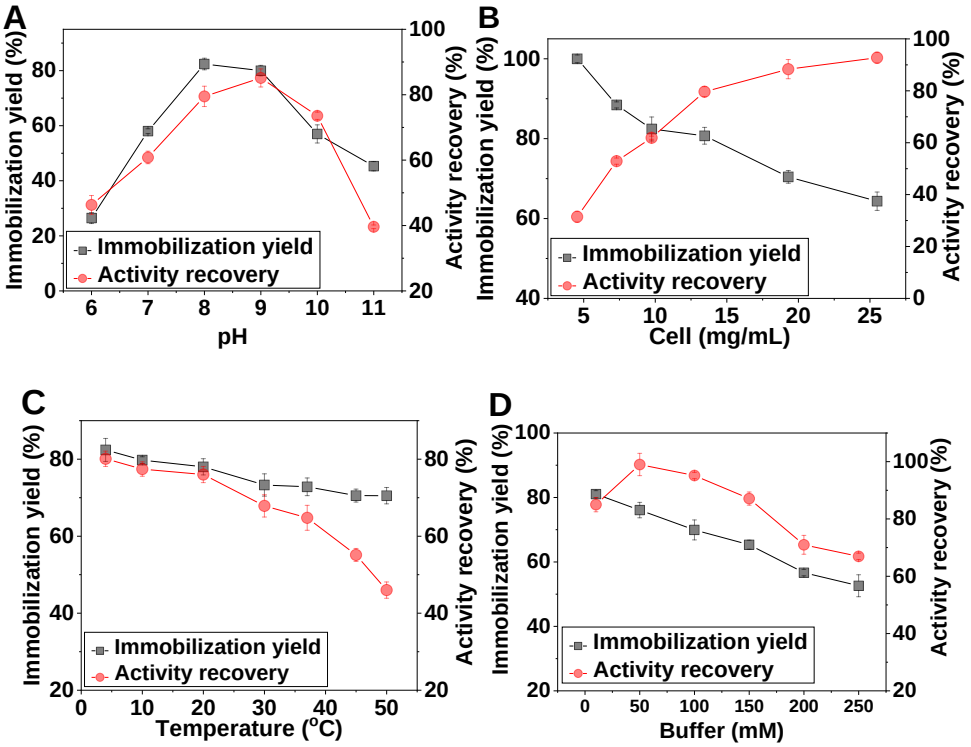

Figure 3. Effect of (**A**) pH, (**B**) cell concentration, (**C**) temperature, and (**D**) buffer concentration on the immobilization of *E. coli* cells. All the experiments were repeated three times, and the standard deviation was calculated and presented.

2.3. Effect of pH and Temperature on the Free and Immobilized Cells

The characteristics of the immobilized cells were then compared with those of the free cells. Figure 4A shows the effect of pH on the activity of the free and immobilized *E. coli* cells expressing recombinant glycerol dehydrogenase. The relative activity of the free cells was 75% at pH 6, with the highest value at pH 9.0; then, the activity decreased dramatically to 28.6% at pH 11. Although the immobilized cells showed a similar trend, the optimal pH was 8.0, and the activity slowly decreased to 81% at pH 11, which was 2.9-fold that of the free cells. Obviously, the immobilized cells displayed better activities at pH 10 and 11. The possible reason for the changes is that enhanced rigidity improved stability after immobilization onto the nanoparticles. Also, an alkaline medium (pH 9.0) exerts stress on the metabolic processes of cells. Moreover, the carrier for immobilization also weakens the mass transfer properties and decreases the permeability of *E. coli* cells [49,50]. Accordingly, the optimum pH for the immobilized cells shifted to 9.0. Additionally, the immobilized cells retained more than 60% residual activity at pH 6–11, whereas in comparison, the free cells exhibited only 14.4% activity at pH 11.0.

The effects of temperature on the activity of free and immobilized cells at pH 8.0 over the range 30 to 90 °C were checked. As shown in Figure 4B, the catalytic activities of the immobilized and free cells were both maximal at 50 °C. The reason for this might be that an increase in the temperature favored the accelerated movement of the cells, resulting in enhanced activity. However, as the temperature

increased further, the secondary structures of the enzymes inside the cell could be disrupted, resulting in decreased activity. Compared with the free cells, immobilization restricted the inactivation of the cells. Thus, when the temperature increased to 90 °C, the free cells retained only 10.56% of their activity, while the immobilized cells retained more than 45% of their activity.

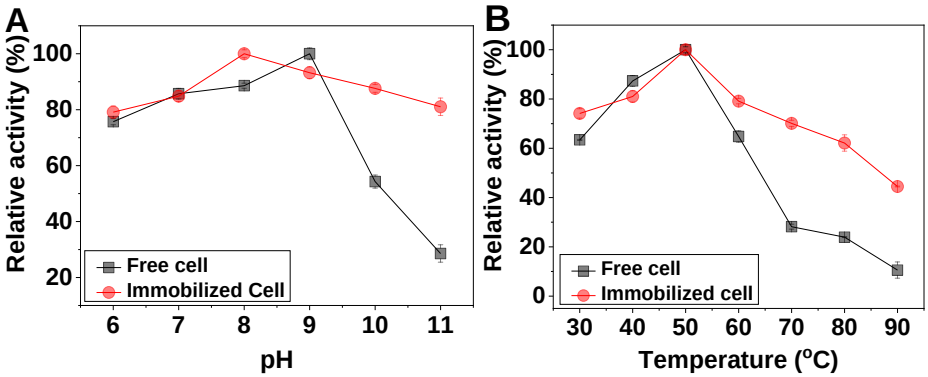

Figure 4. Effects of (**A**) pH and (**B**) temperature on the activities of the free and immobilized cells. All the experiments were repeated three times, and the standard deviation was calculated and presented as error bars.

2.4. Thermal Stability and Reusability of the Free and Immobilized Cells

The thermal stability of a cell is one of the most important properties for their industrial application [51]. The thermal stability of the free and immobilized cells was tested at 37 °C. It was clearly shown that the activity of the free cells decreased rapidly at 37 °C over a 0.5–3 h incubation, whereas the activity of the immobilized cells declined slowly. After incubation at 37 °C for 3 h, only 34% of the initial enzyme activity remained in the free cells, whereas the immobilized cells retained more than 87% of their initial enzyme activity. Moreover, the activity retention in the immobilized cell was 10 times higher than for the free cells after incubation at 37 °C for 3 h. These results demonstrated that after immobilization, the cells had better thermal stability. This may be due to solid-phase carriers protecting the enzyme molecules from external high temperatures, thereby enhancing the enzyme's thermal stability [52].

The reusability of the immobilized cells was also studied. As shown in Figure 5B, the immobilized cells had a higher degree of stability. After five cycles, the immobilized cells retained 70% of their initial activity, while the free cells retained only 10%. Moreover, the immobilized cells retained about 50% of their initial activity after 10 cycles. These results revealed that the immobilized cells had good operational stability and thermostability, which could lower the costs of industrial applications [53].

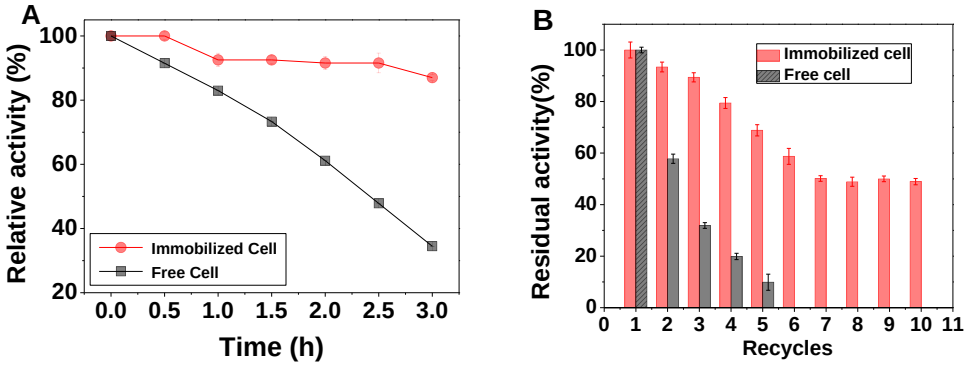

Figure 5. Thermal stability and reusability. (**A**) Thermal stability of the free and immobilized cells. (**B**) Reusability of the immobilized cells. All the experiments were repeated three times, and the standard deviation was calculated and presented as error bars.

2.5. Synthesis of 1,3-Dihydroxyacetone (DHA)

DHA is widely used in the cosmetic industry to produce artificial suntan lotion. The opportunity to produce DHA from glycerol is of particular interest due to the large surplus of glycerol that is formed as a by-product in the biodiesel industry [54]. To assess the possible industrial applications of the immobilized whole cells, the bioconversion of glycerol to DHA was carried out as a proof of concept. Immobilized cells harboring the glycerol dehydrogenase gene were selected for the synthesis of DHA. The time course of the conversion process is shown in Figure 6. After 12 h, approximately 7.5 mM DHA was produced by the immobilized cells, showing a two-fold improvement in the conversion rate compared with the free cells (3.48 mM DHA). Although the product inhibition still had an adverse effect on the system, the yield of DHA showed a relevant enhancement in comparison to previous studies [52]. Moreover, the immobilization method utilized in this study did not require enzyme purification and expensive cofactors. Therefore, it can reduce expenses significantly.

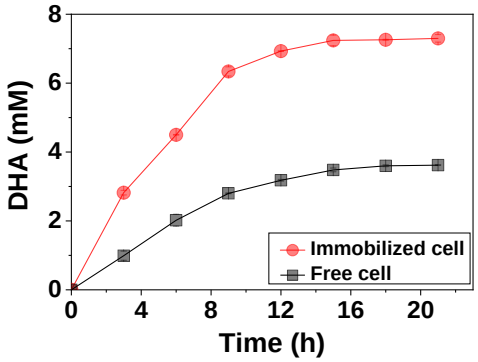

Figure 6. Time course of the synthesis 1,3-dihydroxyacetone (DHA) with immobilized cells. All the experiments were repeated three times, and the standard deviation was calculated and presented as error bars.

3. Materials and Methods

3.1. Materials

$FeSO_4 \cdot 7H_2O$, $FeCl_3 \cdot 6H_2O$, tryptone, oleic acid, glycerol sodium chloride, and yeast extract were from Sinopharm (Shanghai, China). Isopropyl-thio-β- D-galactoside (IPTG), kanamycin, and dopamine hydrochloride were all purchased from Sigma (St. Louis, MO, USA). D-mannosamine hydrochloride was obtained from Yuanye (Shanghai, China) Biotechnology Co. Ltd. Unless otherwise stated, all chemicals and reagents were commercial analytical- or biological-grade.

3.2. Preparation of Magnetic Nanocarriers Functionalized with Mannose

The preparation of magnetic nanocarrier Fe_3O_4@OA@DP was conducted in our previous report [3]. Mannose functionalization of this nanocarrier was performed using the following procedure: typically, 1.0 g of Fe_3O_4@OA@DP nanoparticles was dissolved in 100 mL of citrate buffer (10 mM, pH 4.0). Following this, D-mannosamine hydrochloride (0.23 g) was added to the solution, and the reaction mixture was stirred continuously for 3 h. The material was collected by magnetic separation and washed with deionized water. The product was dried for 12 h at 50 °C and is referred to as Fe_3O_4OA@DP-mannose.

3.3. Characterization of the Magnetic Nanoparticles

The morphologies of Fe_3O_4@OA@DP and Fe_3O_4@OA@DP–mannose nanoparticles were observed by TEM, (Tecnai 12, Philips FEI, Amsterdam, Netherlands). To do this, a few drops of a dilute sample

of each of the nanoparticles were placed on a carbon-coated copper grid and dried overnight at room temperature before analysis.

The chemical structure and functional groups presented in the Fe_3O_4@OA@DP–mannose nanoparticles were examined using an FTIR spectrophotometer (PARAGON 500, Perkin Elmer, Waltham, MA, USA). The samples were dried at 80 °C and compressed with KBr. Spectra were recorded twice at a resolution of 4 cm^{-1}.

3.4. Immobilization of E. coli Cells onto the Fe_3O_4@OA@DP–Mannose Nanoparticles

E. coli cells expressing recombinant glycerol dehydrogenase were prepared in our previous work [55]. Immobilization of the *E. coli* cells was carried out as follows: the mannose-functionalized nanoparticles (30 mg) were added to PBS buffer (10 mM, pH 7.4) containing 1 mM Mn^{2+} and 1 mM Ca^{2+} and the *E. coli* cells. After incubation for 2 h at 4 °C with gentle shaking, the samples were separated by magnetic force and washed two times with deionized water. The immobilization yield (Y%) and the activity recovery (E%) were calculated as follows:

$$Y\% = 100 \times [(R0-R1-R2)/R0]; E\% = 100 \times (A1/A0)$$

where R0 refers to the original optical density at 600 nm (OD_{600}) of the cell suspension, R1 refers to the OD_{600} of the suspension after immobilization and magnetic separation, R2 is the OD_{600} of the washing solution after magnetic separation, A0 is the total activity of the immobilized cells, and A1 is the total activity of the free cells.

3.5. Desorption of E. coli from the Fe_3O_4@OA@DP–Mannose Nanoparticles

Desorption of *E. coli* from the Fe_3O_4@OA@DP–mannose nanoparticles was performed as follows: the immobilized cells were collected using a magnetic field and added into PBS (pH 8.0) containing 1 mM Mn^{2+}, 1 mM Ca^{2+}, and 100 mM D-mannose. The mixture was incubated at 4 °C for 1 h with gentle shaking. The cells desorption rate was calculated by monitoring the increase of OD_{600} of the suspensions.

3.6. Activity Assay

The biological activity of *E. coli* was assessed using the harbored glycerol dehydrogenase, as previously described [3]. The activity was measured by the biocatalytic conversion of glycerol to 1,3-dihydroxyacetone (DHA). The reaction mixture (1 mL final volume) contained glycerol (100 mM, final concentration), 30 mg immobilized cells, or 2 mL (16 mg/mL) of fresh cell suspension, and PBS buffer (10 mM, pH 8.0). After a reaction lasting 5 min, the free or immobilized cells were separated by centrifugation respectively, and the DHA production was analyzed spectrophotometrically using the diphenylamine chromogenic method [56]. One unit of activity (U) was defined as the amount of DHA that can be released per gram of cells per minute under the assay conditions.

3.7. Effect of Buffer Concentration, pH, and Temperature on the Cells

The effect of buffer concentration on the activities of the free and immobilized cells was investigated over the concentration range 10 to 200 mM. All substrate mixtures used contained phosphate buffer at pH 8.0 at 25 °C. Every experiment was repeated in triplicate, and the standard deviation was also calculated. The activities of the immobilized and free cells were also measured at different pHs to determine the effect of pH on the cells. The buffers used in the reactions were the following: 0.2 M sodium carbonate buffer solution (pH 10.0 and 11.0), 0.2 M Tris-HCl solution (pH 8.0 and 9.0), and 0.2 M PBS (pH 6.0 and 7.0). In addition, the substrate was dissolved in 50 mM PBS at 25 °C. The effect of temperature on the activity of the free and immobilized cells was also investigated. The activities of the free and immobilized cells were determined over different temperatures ranging from 30 to 80 °C at intervals of 10 °C. The substrate solution was dissolved in 50 mM phosphate buffer (pH 8.0).

3.8. Thermal Stability and Reusability of the Immobilized Cells

Thermal stability was investigated by monitoring the remaining activity of the free and immobilized cells in a water bath at 37 °C for different times, ranging from 0.5 to 3.0 h, and then measuring the residual activity. The reusability of the immobilized cells was also investigated by the repeated use of the immobilized cells to catalyze the conversion of the substrate. The activity obtained after each round of use was compared with the initial activity to calculate the relative activity. Between two consecutive reactions, the cells were separated from the reaction media by centrifugation, washed with the 0.2 M PBS (pH 8.0), and then added to the new substrate solutions to start a new reaction. Each experiment was repeated in triplicate to minimize errors.

3.9. Synthesis of 1,3-Dihydroxyacetone (DHA) with the Immobilized Cells

The synthesis of DHA was performed with the immobilized cells using glycerol as the substrate. The total volume of the reaction system was set at 5 mL, and the final substrate concentration was 0.8 M. The reaction was carried out in phosphate buffer (pH 8.0) at 25 °C. DHA concentration was analyzed using the diphenylamine chromogenic method.

4. Conclusions

In summary, a unique method for the immobilization of *E. coli* cells expressing recombinant glycerol dehydrogenase on mannose-modified magnetic Fe_3O_4@OA@DP nanoparticles, based on the specific recognition of mannose by FimH, was developed. Because of the superparamagnetism of magnetic nanoparticles, the immobilized cells could be recycled easily under a magnetic field. The immobilized cells had a higher thermal stability and reusability than the free cells. Moreover, the immobilized cells demonstrate a promising future for producing 1,3-DHA; in fact, they produced 1,3-DHA at two times the rate of the free cells. Thus, mannose-functionalized magnetic nanoparticles have a promising industrial potential, and furthermore, this method could be used to recognize and label bacteria.

Author Contributions: F.-L.L. and M.-Y.Z. analyzed the data and wrote the manuscript; F.-L.L., M.-Y.Z., J.-J.S., X.-M.F. and H.C. performed the experiments; Y.-W.Z. and J.-K.L. designed the experiments and reviewed the manuscript. All authors read and approved the final manuscript.

Funding: This work was supported by the Ministry of Science, ICT and Future Planning, Republic of Korea (2013M3A6A8073184, NRF-2017R1A2B3011676, NRF-2017R1A4A1014806).

Conflicts of Interest: The authors declare that they have no competing interests.

References

1. Matsumoto, T.; Takahashi, S.; Kaieda, M.; Ueda, M.; Tanaka, A.; Fukuda, H.; Kondo, A. Yeast whole-cell biocatalyst constructed by intracellular overproduction of *Rhizopus oryzae* lipase is applicable to biodiesel fuel production. *Appl. Microbiol. Biotechnol.* **2001**, *57*, 515–520. [CrossRef] [PubMed]
2. Patel, S.K.S.; Kumar, V.; Mardina, P.; Li, J.; Lestari, R.; Kalia, V.C.; Lee, J.K. Methanol production from simulated biogas mixtures by co-immobilized *Methylomonas methanica* and *Methylocella tundrae*. *Bioresour. Technol.* **2018**, *263*, 25–32. [CrossRef] [PubMed]
3. Zhuang, M.Y.; Cong, W.; Xu, M.Q.; Ling, X.M.; Shen, J.J.; Zhang, Y.W. Using ConcanavalinA as a Spacer for Immobilization of *E. coli* onto Magnetic Nanoparticles. *Int. J. Biol. Macromol.* **2017**, *104*, 63–69. [CrossRef] [PubMed]
4. Krajčovič, T.; Bučko, M.; Vikartovská, A.; Lacík, I.; Uhelská, L.; Chorvát, D.; Neděla, V.; Tihlaříková, E.; Gericke, M.; Heinze, T.; et al. Polyelectrolyte Complex Beads by Novel Two-Step Process for Improved Performance of Viable Whole-Cell Baeyer-Villiger Monoxygenase by Immobilization. *Catalysts* **2017**, *7*, 353. [CrossRef]
5. Jyoti; Bhatia, K.; Chauhan, K.; Attri, C.; Seth, A. Improving stability and reusability of *Rhodococcus pyridinivorans* NIT-36 nitrilase by whole cell immobilization using chitosan. *Int. J. Biol. Macromol.* **2017**, *103*, 8–15. [CrossRef] [PubMed]

6. Patel, S.K.S.; Choi, S.H.; Kang, Y.C.; Lee, J.-K. Eco-Friendly Composite of Fe_3O_4-Reduced Graphene Oxide Particles for Efficient Enzyme Immobilization. *ACS Appl. Mater. Interfaces* **2017**, *9*, 2213–2222. [CrossRef] [PubMed]
7. Kim, T.-S.; Patel, S.K.S.; Selvaraj, C.; Jung, W.-S.; Pan, C.-H.; Kang, Y.C.; Lee, J.-K. A highly efficient sorbitol dehydrogenase from *Gluconobacter oxydans G624* and improvement of its stability through immobilization. *Sci. Rep.* **2016**, *6*, 33438. [CrossRef] [PubMed]
8. Patel, S.K.S.; Singh, R.K.; Kumar, A.; Jeong, J.-H.; Jeong, S.H.; Kalia, V.C.; Kim, I.-W.; Lee, J.-K. Biological methanol production by immobilized *Methylocella tundrae* using simulated biohythane as a feed. *Bioresour. Technol.* **2017**, *241*, 922–927. [CrossRef]
9. Patel, S.K.S.; Kondaveeti, S.; Otari, S.V.; Pagolu, R.T.; Jeong, S.H.; Kim, S.C.; Cho, B.-K.; Kang, Y.C.; Lee, J.-K. Repeated batch methanol production from a simulated biogas mixture using immobilized *Methylocystis bryophila*. *Energy* **2018**, *145*, 477–485. [CrossRef]
10. Patel, S.K.S.; Kumar, P.; Singh, M.; Lee, J.-K.; Kalia, V.C. Integrative approach to produce hydrogen and polyhydroxybutyrate from biowaste using defined bacterial cultures. *Bioresour. Technol.* **2015**, *176*, 136–141. [CrossRef]
11. Yang, L.; Xin, J.; Zhang, Z.; Yan, H.; Wang, J.; Sun, E.; Hou, J.; Jia, X.; Lv, H. TPGS-modified liposomes for the delivery of ginsenoside compound K against non-small cell lung cancer: Formulation design and its evaluation in vitro and in vivo. *J. Pharm. Pharmacol.* **2016**, *68*, 1109–1118. [CrossRef]
12. Wu, Y.-S.; Ngai, S.-C.; Goh, B.-H.; Chan, K.-G.; Lee, L.-H.; Chuah, L.-H. Anticancer Activities of Surfactin and Potential Application of Nanotechnology Assisted Surfactin Delivery. *Front. Pharmacol.* **2017**, *8*. [CrossRef] [PubMed]
13. Rui, M.; Xin, Y.; Li, R.; Ge, Y.; Feng, C.; Xu, X. Targeted Biomimetic Nanoparticles for Synergistic Combination Chemotherapy of Paclitaxel and Doxorubicin. *Mol. Pharm.* **2017**, *14*, 107–123. [CrossRef] [PubMed]
14. Ali, S.; Morsy, R.; El-Zawawy, N.; Fareed, M.; Bedaiwy, M. Synthesized zinc peroxide nanoparticles (ZnO_2-NPs): A novel antimicrobial, anti-elastase, anti-keratinase, and anti-inflammatory approach toward polymicrobial burn wounds. *Int. J. Nanomed.* **2017**, *12*, 6059–6073. [CrossRef]
15. Wang, G.; Wang, J.J.; Chen, X.L.; Du, L.; Li, F. Quercetin-loaded freeze-dried nanomicelles: Improving absorption and anti-glioma efficiency in vitro and in vivo. *J. Controll. Release* **2016**, *235*, 276–290. [CrossRef]
16. Shi, F.; Zhao, Y.; Firempong, C.K.; Xu, X. Preparation, characterization and pharmacokinetic studies of linalool-loaded nanostructured lipid carriers. *Pharm. Biol.* **2016**, *54*, 2320–2328. [CrossRef]
17. Peng, W.; Jiang, X.; Zhu, Y.; Omari-Siaw, E.; Deng, W.; Yu, J.; Xu, X.; Zhang, W. Oral delivery of capsaicin using MPEG-PCL nanoparticles. *Acta Pharmacol. Sin.* **2015**, *36*, 139–148. [CrossRef]
18. Zhang, H.; Firempong, C.K.; Wang, Y.; Xu, W.; Wang, M.; Cao, X.; Zhu, Y.; Tong, S.; Yu, J.; Xu, X. Ergosterol-loaded poly(lactide-co-glycolide) nanoparticles with enhanced in vitro antitumor activity and oral bioavailability. *Acta Pharmacol. Sin.* **2017**, *37*, 834–844. [CrossRef] [PubMed]
19. Kim, J.; Grate, J.W.; Wang, P. Nanostructures for enzyme stabilization. *Chem. Eng. Sci.* **2006**, *61*, 1017–1026. [CrossRef]
20. Xiong, F.; Hu, K.; Yu, H.; Zhou, L.; Song, L.; Zhang, Y.; Shan, X.; Liu, J.; Gu, N. A Functional Iron Oxide Nanoparticles Modified with PLA-PEG-DG as Tumor-Targeted MRI Contrast Agent. *Pharm. Res.* **2017**, *34*, 1683–1692. [CrossRef]
21. Shen, S.; Wu, L.; Liu, J.; Xie, M.; Shen, H.; Qi, X.; Yan, Y.; Ge, Y.; Jin, Y. Core–shell structured Fe_3O_4@TiO_2-doxorubicin nanoparticles for targeted chemo-sonodynamic therapy of cancer. *Int. J. Pharm.* **2015**, *486*, 380–388. [CrossRef] [PubMed]
22. Kilonzo, P.; Margaritis, A.; Bergougnou, M. Effects of surface treatment and process parameters on immobilization of recombinant yeast cells by adsorption to fibrous matrices. *Bioresour. Technol.* **2011**, *102*, 3662–3672. [CrossRef] [PubMed]
23. Zhang, Y.W.; Prabhu, P.; Lee, J.K. Alginate immobilization of recombinant *Escherichia coli* whole cells harboring L-arabinose isomerase for L-ribulose production. *Bioprocess Biosyst. Eng.* **2010**, *33*, 741–748. [CrossRef] [PubMed]
24. Ayer, M.; Klok, H.A. Cell-mediated delivery of synthetic nano- and microparticles. *J. Controll. Release* **2017**. [CrossRef] [PubMed]

25. Ni, K.; Lu, H.; Wang, C.; Black, K.C.; Wei, D.; Ren, Y.; Messersmith, P.B. A novel technique for *in situ* aggregation of *Gluconobacter oxydans* using bio-adhesive magnetic nanoparticles. *Biotechnol. Bioeng.* **2012**, *109*, 2970–2977. [CrossRef] [PubMed]
26. Zhang, Z.; Huang, J.; Jiang, S.; Liu, Z.; Gu, W.; Yu, H.; Li, Y. Porous starch based self-assembled nano-delivery system improves the oral absorption of lipophilic drug. *Int. J. Pharm.* **2013**, *444*, 162–168. [CrossRef] [PubMed]
27. Akashi, M.; Maruyama, I.; Fukudome, N.; Yashima, E. Immobilization of human thrombomodulin on glass beads and its anticoagulant activity. *Bioconj. Chem.* **1992**, *3*, 363. [CrossRef]
28. Guedri, H.; Durrieu, C. A self-assembled monolayers based conductometric algal whole cell biosensor for water monitoring. *Microchim. Acta* **2008**, *163*, 179–184. [CrossRef]
29. Chouteau, C.; Dzyadevych, S.; Durrieu, C.; Chovelon, J.M. A bi-enzymatic whole cell conductometric biosensor for heavy metal ions and pesticides detection in water samples. *Biosens. Bioelectron.* **2005**, *21*, 273–281. [CrossRef]
30. Lagarde, F.; Jaffrezic-Renault, N. Cell-based electrochemical biosensors for water quality assessment. *Anal. Bioanal. Chem.* **2011**, *400*, 947. [CrossRef]
31. Miller, E.; Garcia, T.; Hultgren, S.; Oberhauser, A.F. The mechanical properties of *E. coli* type 1 pili measured by atomic force microscopy techniques. *Biophys. J.* **2006**, *91*, 3848–3856. [CrossRef] [PubMed]
32. Li, H.; Dong, W.; Zhou, J.; Xu, X.; Li, F. Triggering effect of N-acetylglucosamine on retarded drug release from a lectin-anchored chitosan nanoparticles-in-microparticles system. *Int. J. Pharm.* **2013**, *449*, 37–43. [CrossRef]
33. Yazgan, I.; Noah, N.M.; Toure, O.; Zhang, S.; Sadik, O.A. Biosensor for selective detection of *E. coli* in spinach using the strong affinity of derivatized mannose with fimbrial lectin. *Biosens. Bioelectron.* **2014**, *61*, 266–273. [CrossRef]
34. Yang, W.; Pan, C.Y.; Luo, M.D.; Zhang, H.B. Fluorescent mannose-functionalized hyperbranched poly(amido amine)s: Synthesis and interaction with *E. coli*. *Biomacromolecules* **2010**, *11*, 1840–1846. [CrossRef] [PubMed]
35. Zhuang, M.Y.; Zhou, Q.L.; Wang, X.Y.; Zhang, J.X.; Xue, L.; Wang, R.; Zhang, J.X.; Zhang, Y.W. Immobilization of Lipase Onto Dopamine Functionalized Magnetic Nanoparticles. *Nanosci. Nanotechnol. Lett.* **2016**, *8*, 251–254. [CrossRef]
36. Klemm, P.; Jørgensen, B.J.; Die, I.V.; Han, D.R.; Bergmans, H. The fim genes responsible for synthesis of type 1 fimbriae in *Escherichia coli*, cloning and genetic organization. *Mol. Gen. Genet. MGG* **1985**, *199*, 410. [CrossRef]
37. Klemm, P.; Christiansen, G. Three FIM genes required for the regulation of length and mediation of adhesion of *Escherichia coli* type 1 fimbriae. *Mol. Gen. Genet. MGG* **1987**, *208*, 439–445. [CrossRef] [PubMed]
38. Krogfelt, K.A.; Bergmans, H.; Klemm, P. Direct evidence that the FimH protein is the mannose-specific adhesin of *Escherichia coli* type 1 fimbriae. *Infect. Immun.* **1990**, *58*, 1995–1998. [CrossRef]
39. Aprikian, P.; Tchesnokova, V.; Kidd, B.; Yakovenko, O.; Yarov-Yarovoy, V.; Trinchina, E.; Vogel, V.; Thomas, W.; Sokurenko, E. Interdomain Interaction in the FimH Adhesin of *Escherichia coli* Regulates the Affinity to Mannose. *J. Biol. Chem.* **2007**, *282*, 23437. [CrossRef] [PubMed]
40. Möckl, L.; Fessele, C.; Despras, G.; Bräuchle, C.; Lindhorst, T.K. En route from artificial to natural: Evaluation of inhibitors of mannose-specific adhesion of *E. coli* under flow. *Biochim. Biophys. Acta* **2016**, *1860*, 2031–2036. [CrossRef] [PubMed]
41. Liu, W.; Zhou, F.; Zhang, X.-Y.; Li, Y.; Wang, X.-Y.; Xu, X.-M.; Zhang, Y.-W. Preparation of Magnetic Fe_3O_4@SiO_2 Nanoparticles for Immobilization of Lipase. *J. Nanosci. Nanotechnol.* **2014**, *14*, 3068–3072. [CrossRef]
42. Liu, C.H.; Li, X.Q.; Jiang, X.P.; Zhuang, M.Y.; Zhang, J.X.; Bao, C.H.; Zhang, Y.W. Preparation of Functionalized Graphene Oxide Nanocomposites for Covalent Immobilization of NADH Oxidase. *Nanosci. Nanotechnol. Lett.* **2016**, *8*, 164–167. [CrossRef]
43. Tao, Q.-L.; Li, Y.; Shi, Y.; Liu, R.-J.; Zhang, Y.-W.; Guo, J. Application of Molecular Imprinted Magnetic Fe_3O_4@SiO_2 Nanoparticles for Selective Immobilization of Cellulase. *J. Nanosci. Nanotechnol.* **2016**, *16*, 6055–6060. [CrossRef] [PubMed]
44. Shi, Y.; Liu, W.; Tao, Q.-L.; Jiang, X.P.; Liu, C.-H.; Zeng, S.; Zhang, Y.-W. Immobilization of Lipase by Adsorption onto Magnetic Nanoparticles in Organic Solvents. *J. Nanosci. Nanotechnol.* **2016**, *16*, 601–607. [CrossRef] [PubMed]

45. Rambaud, C.; Oppenländer, A.; Trommsdorff, H.P.; Vial, J.C. Tunneling dynamics of delocalized protons in hydrogen bonds at low temperatures. *J. Lumin.* **1990**, *45*, 310–312. [CrossRef]
46. Liu, F.; Kozlovskaya, V.; Zavgorodnya, O.; Martinezlopez, C.; Catledge, S.; Kharlampieva, E. Encapsulation of anticancer drug by hydrogen-bonded multilayers of tannic acid. *Soft Matter* **2014**, *10*, 9237. [CrossRef]
47. Sharon, N. Carbohydrates as future anti-adhesion drugs for infectious diseases. *Biochim. Biophys. Acta BBA Gen. Subj.* **2006**, *1760*, 527–537. [CrossRef]
48. Hung, C.-S.; Bouckaert, J.; Hung, D.; Pinkner, J.; Widberg, C.; DeFusco, A.; Auguste, C.G.; Strouse, R.; Langermann, S.; Waksman, G.; et al. Structural basis of tropism of *Escherichia coli* to the bladder during urinary tract infection: FimH mannose-binding pocket. *Mol. Microbiol.* **2002**, *44*, 903–915. [CrossRef]
49. Yang, H.; Shen, Y.; Xu, Y.; Maqueda, A.S.; Zheng, J.; Wu, Q.; Tam, J. A novel strategy for the discrimination of gelatinous Chinese medicines based on enzymatic digestion followed by nano-flow liquid chromatography in tandem with orbitrap mass spectrum detection. *Int. J. Nanomed.* **2015**, 4947–4955. [CrossRef]
50. Man, R.C.; Ismail, A.F.; Fuzi, S.F.Z.M.; Ghazali, N.F.; Illias, R.M. Effects of Culture Conditions of Immobilized Recombinant *Escherichia coli* on Cyclodextrin Glucanotransferase (CGTase) Excretion and Cell Stability. *Process Biochem.* **2016**, *51*, 474–483. [CrossRef]
51. Zhang, Y.-W.; Jeya, M.; Lee, J.-K. L-Ribulose production by an *Escherichia coli* harboring l-arabinose isomerase from *Bacillus licheniformis*. *Appl. Microbiol. Biotechnol.* **2010**, *87*, 1993–1999. [CrossRef]
52. Zhang, Y.; Gao, F.; Zhang, S.P.; Su, Z.G.; Ma, G.H.; Wang, P. Simultaneous production of 1,3-dihydroxyacetone and xylitol from glycerol and xylose using a nanoparticle-supported multi-enzyme system with in situ cofactor regeneration. *Bioresour. Technol.* **2011**, *102*, 1837–1843. [CrossRef] [PubMed]
53. Singh, R.K.; Zhang, Y.W.; Nguyen, N.P.T.; Jeya, M.; Lee, J.K. Covalent immobilization of β-1,4-glucosidase from *Agaricus arvensis* onto functionalized silicon oxide nanoparticles. *Appl. Microbiol. Biotechnol.* **2011**, *89*, 337–344. [CrossRef] [PubMed]
54. Jiang, X.P.; Lu, T.T.; Liu, C.H.; Ling, X.M.; Zhuang, M.Y.; Zhang, J.X.; Zhang, Y.W. Immobilization of dehydrogenase onto epoxy-functionalized nanoparticles for synthesis of (R)-mandelic acid. *Int. J. Biol. Macromol.* **2016**, *88*, 9–17. [CrossRef] [PubMed]
55. Zhuang, M.Y.; Jiang, X.P.; Ling, X.-M.; Xu, M.-Q.; Zhu, Y.-H.; Zhang, Y.W. Immobilization of glycerol dehydrogenase and NADH oxidase for enzymatic synthesis of 1,3-dihydroxyacetone with *in situ* cofactor regeneration. *J. Chem. Technol. Biotechnol.* **2018**, *93*, 2351–2358. [CrossRef]
56. Zhou, Y.J.; Yang, W.; Wang, L.; Zhu, Z.; Zhang, S.; Zhao, Z.K. Engineering NAD^+ availability for *Escherichia coli* whole-cell biocatalysis: A case study for dihydroxyacetone production. *Microb. Cell Fact.* **2013**, *12*, 103. [CrossRef]